



# Structurally stable electrospun nanofibrous cellulose acetate/chitosan biocomposite membranes for the removal of chromium ions from the polluted water

Jinhui Xiong<sup>1</sup> · Qian Hu<sup>1</sup> · Jiayi Wu<sup>1</sup> · Zhiwen Jia<sup>1</sup> · Shengbo Ge<sup>1,2</sup> · Yizhong Cao<sup>3</sup> · Juying Zhou<sup>4</sup> · Yaxin Wang<sup>1</sup> · Jinsong Yan<sup>1</sup> · Linkun Xie<sup>1</sup> · Xijuan Chai<sup>1</sup> · Lianpeng Zhang<sup>1</sup> · Guanben Du<sup>1</sup> · Siqun Wang<sup>5</sup> · Kaimeng Xu<sup>1</sup>

Received: 11 February 2023 / Revised: 15 April 2023 / Accepted: 26 April 2023 / Published online: 13 May 2023  
© The Author(s), under exclusive licence to Springer Nature Switzerland AG 2023

## Abstract

Cellulose acetate (CA) and chitosan (CS) were selected as the raw materials for preparing the biobased porous nanofibers for the removal of chromium ions in aqueous solutions. The structurally stable nanofibrous biocomposite membranes were successfully electrospun fabricated using a double-needle method. Nanoindentation mapping revealed that the micro or nano-scale knots were formed through a synergistic action of the hydrogen bonding, electrostatic forces, and interfacial compatibility of CA and CS. The average elastic modulus and hardness values of CA/CS biocomposite nanofibers were 0.23 GPa and 1.72 GPa, respectively. The nanofibrous membrane exhibited outstanding structural stability in an aqueous solution (with a wide pH range) and good thermal stability. The biocomposite nanofibrous membrane with 50% CS loading (BENF-50) had an optimum adsorption capacity of 51.6 mg/g for chromium ions in the aqueous solution at pH=3 as well as good reusability of up to eight cycles. The fabricated biocomposite nanofibrous membranes showed excellent structural stability, thermal stability, and adsorption performance, making them promising adsorbent materials for treating water pollution.

**Keywords** Electrospinning · Nanofibrous membrane · Structural stability · Adsorption · Chromium ion

## 1 Introduction

The rapid development of global industrialization and the overuse of fossil energy lead to the deterioration of environmental pollution [1, 2]. Heavy metals are considered as the major pollutants in aquatic ecosystems produced from

both natural and industrial sources [3, 4]. The naturally produced heavy metals are originated from the erosion of metal-containing rocks and the release of a volcanic eruption [5]. The industrially produced heavy metal pollutants are from sewage irrigation, municipal wastes, mining wastes, machinery manufacturing, and electroplating [6, 7]. Additionally, heavy metal pollutants can be generated from fertilizers and pesticides used in agricultural production. A recent survey of the famous scenery of the Lijiang River

Jinhui Xiong, Qian Hu, and Jiayi Wu contributed equally to this work.

✉ Shengbo Ge  
geshengbo@njfu.edu.cn

✉ Lianpeng Zhang  
lpz@zju.edu.cn

✉ Kaimeng Xu  
xukm007@163.com

<sup>1</sup> Yunnan Provincial Key Laboratory of Wood Adhesives and Glued Products, International Joint Research Center for Biomass Materials, Southwest Forestry University, Kunming 650224, China

<sup>2</sup> Jiangsu Co-Innovation Center of Efficient Processing and Utilization of Forest Resources, International Innovation

Center for Forest Chemicals and Materials, College of Materials Science and Engineering, Nanjing Forestry University, Nanjing 210037, China

<sup>3</sup> College of Chemistry and Materials Engineering, Zhejiang Agriculture and Forestry University, Hangzhou 311300, China

<sup>4</sup> Key Laboratory of Chemistry and Engineering of Forest Products, Guangxi Key Laboratory of Chemistry and Engineering of Forest Products, State Ethnic Affairs Commission, Guangxi Minzu University, Nanning 530006, China

<sup>5</sup> Center for Renewable Carbon, The University of Tennessee, Knoxville, TN 37996, USA

in China showed that several heavy metal ions including cadmium ( $\text{Cd}^{2+}$ ), chromium ( $\text{Cr}^{6+}$ ), mercury ( $\text{Hg}^{2+}$ ), zinc ( $\text{Zn}^{2+}$ ), and lead ( $\text{Pb}^{2+}$ ) exceeded World Health Organization permissible limit [8–10]. Heavy metals caused severe pollution to aquatic ecosystems, even at the low concentrations. Prolonged accumulation of heavy metals in human bodies through food chains can easily injure some organs, thereby negatively affecting the nervous, reproductive, and cardiovascular systems, leading to carcinogenesis, malformations, and death [11].

Numerous methods, such as precipitation [12], electrolysis [13], photocatalysis [14], separation [15], coagulation/flocculation [16], ion exchange [17], and adsorption [18], have been attempted to mitigate heavy metal pollution. Among these methods, adsorption has gradually become a preferred method, owing to its advantages of facile operation, low cost, nontoxicity, high availability, and good reversibility [19–21]. Electrospun nanofibrous membranes with high porosity, large specific surface area, good permeability, and controllable chemical sorption sites have been considered promising materials for wastewater treatment [22]. The nanofibrous membranes that are modified with various functional groups, such as carboxyl, hydroxyl, amino, and sulfhydryl, have a high adsorption efficiency toward heavy metals. Particularly, the adsorbents containing nitrogen (N) atoms with lone pair electrons can strongly adsorb metal ions through chelation or electrostatic interaction. Chaúque et al. [23] fabricated the amino-functionalized polyacrylonitrile nanofibrous membrane by modifying diethylenetriamine. The membrane exhibited high adsorption capacities for  $\text{Cd}^{2+}$  (32.68 mg/g) and  $\text{Cr}^{6+}$  (66.24 mg/g), respectively.

Eco-friendly and renewable cellulose (CE) displays outstanding physical, mechanical, and stable properties [24, 25]. The lack of functional chemical groups limits the use of cellulose for removing heavy metals. Chitosan (CS), containing inherently rich active functional groups, including hydroxyl and amino groups in molecular chains, can chelate with metal ions; as a result, it has attracted considerable attention in the treatment of water [26, 27]. However, the adsorption performance of CS is low when it is directly used as an adsorbent due to its low specific surface area. Ghaee et al. [28] prepared stable macroporous chitosan membranes by cross-linking of glutaraldehyde and dissolution of silica particles for the adsorption of copper ions ( $\text{Cu}^{2+}$ ). The amino groups in CS became more accessible for chelation after it was cross-linked. Phan et al. [29] fabricated chitosan/cellulose acetate (CS/CA) nanofibers by electrospinning the mixture of CS and CA in a trifluoroacetic/acetic acid co-solvent, followed by a sodium carbonate ( $\text{Na}_2\text{CO}_3$ ) treatment. CS/CA nanofibers had an excellent adsorption capacity of 57.3 and 112.6 mg/g for  $\text{Pb}^{2+}$  and  $\text{Cu}^{2+}$ , respectively. Zia et al. [30] deposited chitosan on poly(L-lactic acid) nanofiber membranes for  $\text{Cu}^{2+}$  adsorption in an aqueous solution. The addition of

chitosan increased the specific surface area of the samples, thus enhancing the action of amino and hydroxyl radicals in chitosan to chelate with  $\text{Cu}^{2+}$ . The maximum adsorption capacity for  $\text{Cu}^{2+}$  can be achieved at  $\text{pH}=7$ . Christou et al. [31] prepared polyvinylpyrrolidone/chitosan nanofibrous membranes to effectively adsorb uranium ( $\text{U}^{6+}$ ) ions in an aqueous solution at  $\text{pH}=6$ . The great adsorption capacity was attributed to the fibrous structure of the material and the amino and hydroxyl groups on chitosan polymers that increased chemical affinity and the formation of inner-sphere complexes between uranium and these surface groups.

To further improve the adsorption performance and reusability of electrospun membranes and to expand their application in industrial wastewater treatment, urban polluted water and air purification, as well as the energy storage, sensor, and phase change materials, it is very necessary to develop the structurally stable porous nanofibrous membranes [32–34]. However, there are few reports on the study of structural stability of electrospun nanofibrous networks. In this study, CA and CS were selected as the raw materials for preparing the biobased porous nanofibers for the removal of chromium ions in wastewater using double and core-shell needles. The structural stability in various pH solutions and the thermal stability of the nanofibrous membrane were investigated. In addition, the effects of contacting time, pH value, and initial concentration of heavy metals on adsorption performance were comparatively studied. Nanoindentation mapping was first introduced to evaluate the nanomechanical properties of the nanofibrous network. The adsorption mechanism of chromium ions on porous nanofibrous membranes was deduced.

## 2 Materials and methods

### 2.1 Materials

CA, 1,5-diphenylcarbonyldihydrazide (DPC), and potassium dichromate were purchased from Sinopharm Chemical Reagent Co., Ltd. CS with a deacetylation degree of 90% was provided by Qingdao Huizhi Biological Engineering Co., Ltd. Glacial acetic acid was bought from Yunnan Huasen Co., Ltd. Polyvinyl alcohol (PVA) was obtained from Shanghai Taitan Technology Co., Ltd.

### 2.2 Fabrication of biocomposite nonfibrous membranes

The CA and CS solutions with optimum concentrations were placed in the different syringes, respectively. The structurally stable CA/CS nanofibrous membranes were fabricated through electrospinning with a double needle (Fig. 1); the composite CA/CS nanofibers with probably

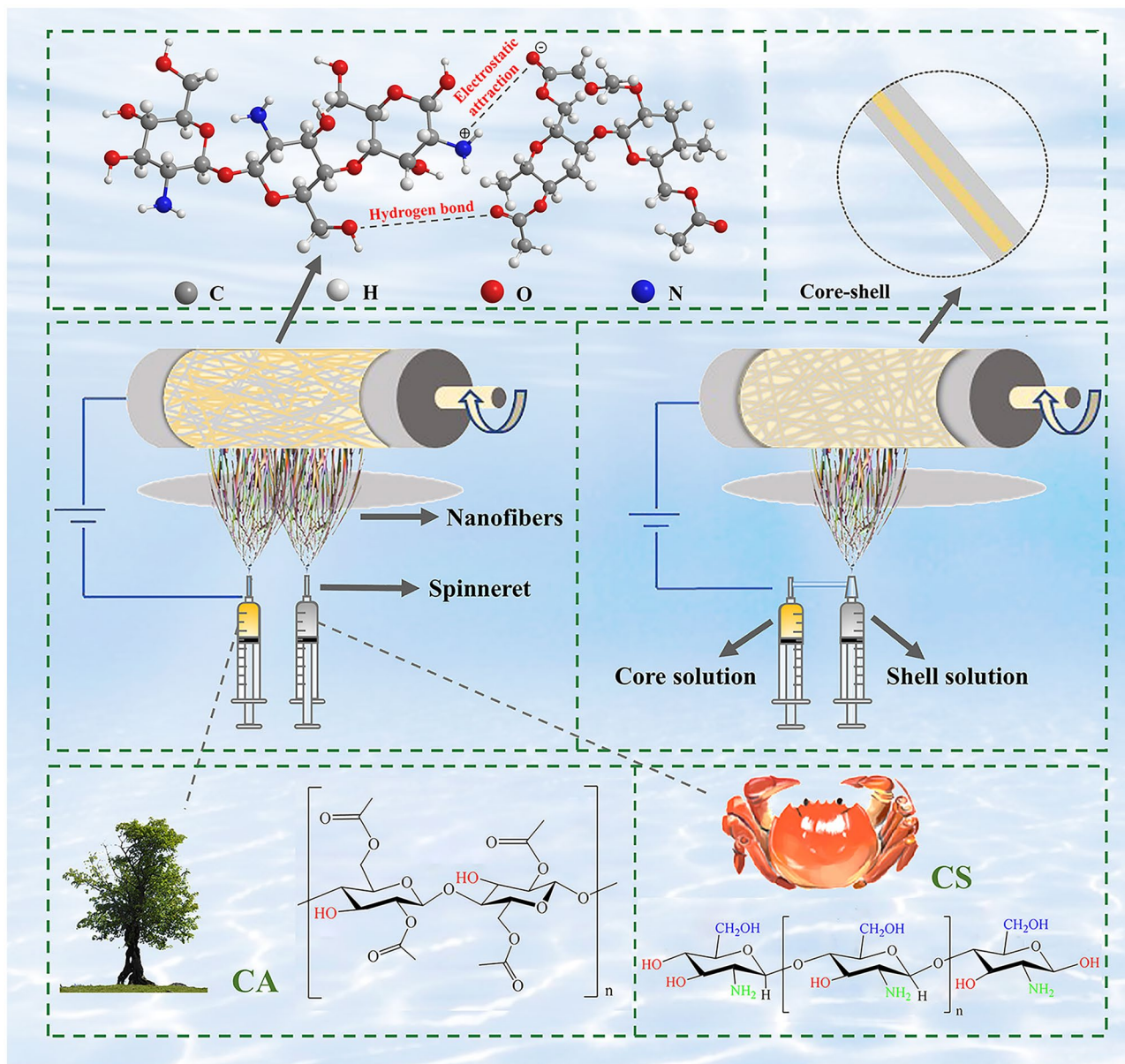


**Fig. 1** Schematic diagram of preparation of electrospun nanofibrous membranes

physical and chemical bonding sites were formed in the high-voltage electrostatic field. The parameters of electrospinning including voltage, injection rate, and collector distance were used according to our previous report [4]. A collector for the nanofibers was wrapped with aluminum foil. The CA/CS biomass electrospun nanofibers with different mass ratios of chitosan of 30%, 50%, and 90% were denoted as BENF-30, BENF-50, and BENF-90, respectively. For further comparative analysis, the core-shell CA/CS electrospun nanofibers were also fabricated at a CS loading of 50%, denoted as core-shell-50.

### 2.3 Characterization of biocomposite nonfibrous membranes

A scanning electron microscope (SEM, Hitachi S-3400, Philips, Japan) was used to observe the micromorphology of nanofibrous membranes. The distribution images of chromium ions after adsorption were obtained using energy-dispersive X-ray spectroscopy (EDS). The three-dimensional shape and roughness of the nanofibrous membranes were examined using an atomic force microscope (AFM, Bruker Multimode 8). The surface

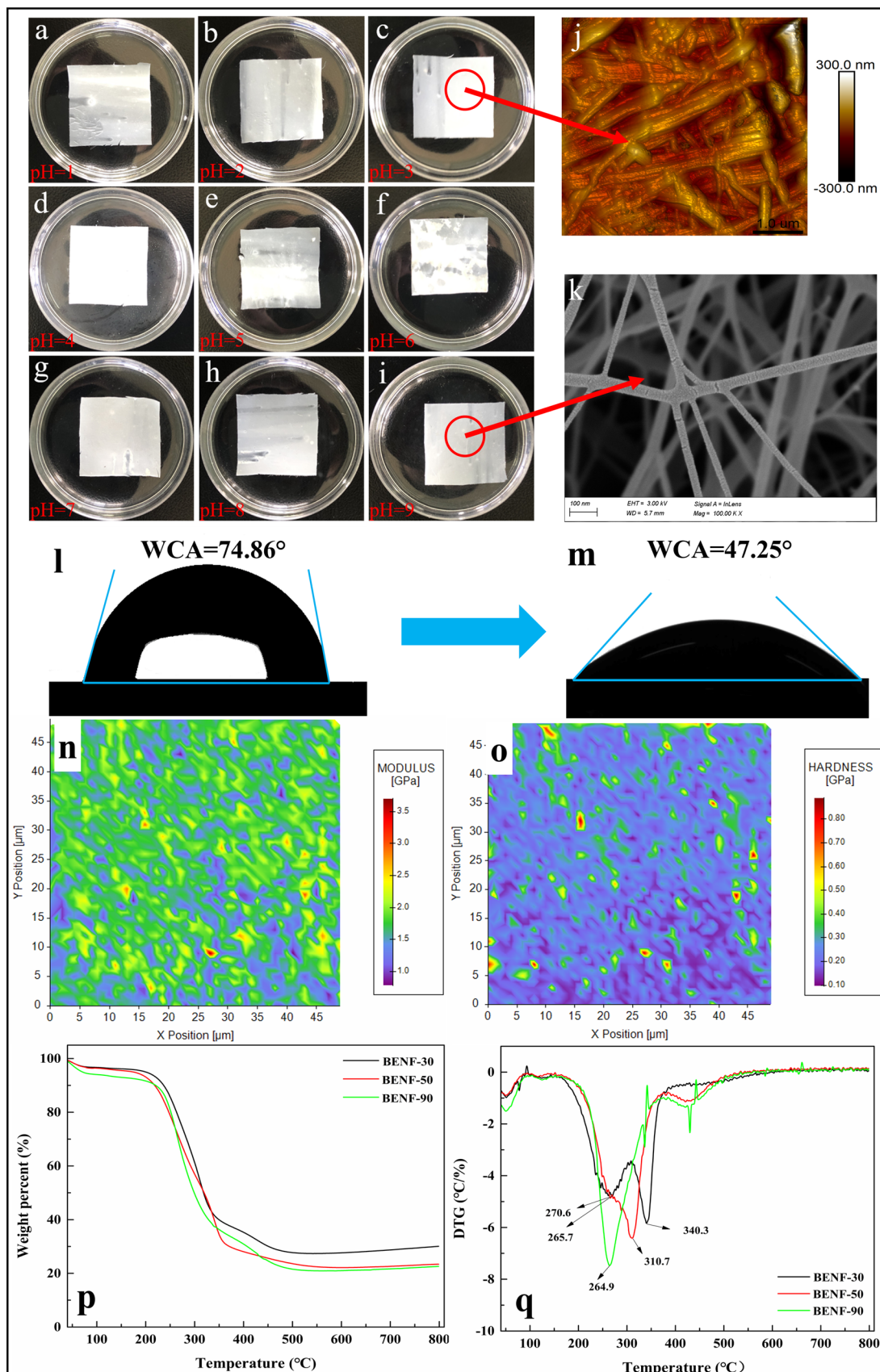


**Fig. 2** The solution stability, wettability, and thermal stability of nanofibrous membranes: **a–i** solution stability in an aqueous environment at various pH; **j, k** AFM and SEM; **l, m** static water contact angles at 0 s and 5 s; **n, o** nano-scale elastic modulus and hardness mapping; **p, q** thermal stability

wettability of the nanofibrous membranes were tested on a static water contact angle (WCA) instrument (JC2000D, Shanghai Zhongcheng Co., Ltd., China). The crystallographic structure of the nanofibrous membranes was examined using an X-ray diffraction (XRD) (Ultima IV, Rigaku, Japan). Fourier-transform-infrared spectroscopy (FTIR) spectra of nanofibrous membranes were obtained using a Nicolet instrument (IS5, Thermo, USA) with the accessory of attenuated total reflectance (ATR). The structural stability of nanofibrous membranes was evaluated using an iMicro nanoindenter (KLA, USA), equipped with a Berkovich indenter with a uniform indent depth in an array referring to the previous reports [35]. The thermal stability of samples was characterized using a thermal gravimetric instrument (TG 209-F1, Netzsch, Germany). The surface chemical compositions were characterized using X-ray photoelectron spectroscopy (XPS) (K-Alpha, Thermo Scientific, USA) with a monochromatic Al-K $\alpha$ .

## 2.4 Adsorption performance of nanofibrous membrane

The absorbance of the samples was measured through the reaction of Cr<sup>6+</sup> with DPC using an ultraviolet–visible (UV–vis) spectrophotometer. The standard curve was used to calculate the adsorption capacity of Cr<sup>6+</sup>. The effects of the adsorption parameters including initial Cr<sup>6+</sup> concentration, contacting time, and pH on the removal of Cr<sup>6+</sup> were investigated. The adsorption capacity of the samples was calculated using Eq. (1).

$$Q = (C_0 - C_t)V/m \quad (1)$$

where  $Q$  is the adsorption capacities, mg/g;  $C_0$  represents the initial concentration of Cr<sup>6+</sup> in the testing solution, mg/L;  $C_t$  is the concentration of Cr<sup>6+</sup> at any time, mg/L;  $V$  indicates the volume of the solution, L;  $m$  is the weight of the nanofibrous membranes, g.

## 3 Results and discussions

### 3.1 Analysis of structural, thermal stability, and wettability

To analyze the structural stability of CA/CS nanofibrous membranes, the BENF-50 was immersed in various

aqueous solutions, with varying pH values ranging from 1 to 9. As shown in Fig. 2b–h, nanofibrous membranes generally were flat and smooth without any damage and dissolution, irrespective of the pH value of the aqueous solution (acid or alkaline). Given the observation in Fig. 2j and k, it was assumed that some micro- or nano-scale knots were probably formed, which were further confirmed by nanoindentation mapping analysis. The formation of micro- or nano-scale knots effectively promoted the stability of CA/CS nanofibrous membranes in the solutions through nanonetwork structures. Some slight shrinkage was observed in the membrane in Fig. 2a and i, which could be attributed to the difference in solubility of polyvinyl alcohol and chitosan and the varieties of surface tension in different pH aqueous solutions. Moreover, the nanofibrous membranes showed the excellent hydrophilicity corresponding to the static water contact angle (WCA) of 74.86° and 47.25° at 0 s and 5 s, respectively, as seen in Fig. 2l and m.

Figure 2p and q displays the thermalgravimetric (TG) and its derivative (DTG) curves of porous nanofibrous membranes. The thermal degradation stages of the samples were mainly divided into three. In the first stage, the evaporation of residual moisture and rupture of weak hydrogen bonds occurred at the temperature range of 40–100 °C, with a slight mass loss of 2 to 5%. The mass loss of the samples significantly increased as the temperature elevated from 100 to 500 °C. The thermal decomposition of the samples at a temperature below 320 °C was due to the breakdown of chemical bond between N-acetylglucosamine rings and the glucosamine on CS, which further decomposed to form acetic, butyric acids, and some fatty acids [36–38]. In the second stage, the thermal decomposition process of CA with the cleavage of glycoside bonds, dehydration, decarboxylation, and decarbonylation occurred at a temperature range of 320–500 °C [39, 40]. In the third stage, the charring of residual CA, CS, and their thermal degradation products occurred at a temperature above 500 °C [41]. The DTG curves showed that the maximum thermal decomposition temperatures ( $T_{max}$ ) at the first stage for BENF-30, BENF-50, and BENF-90 were 270.6, 265.7, and 264.9 °C, respectively, which mainly was attributed to the thermal decomposition of CS. BENF-30 (340.3 °C) exhibited a higher  $T_{max}$  than that of BENF-50 (310.7 °C), owing to the major thermal decomposition of CA. This result showed that the CS addition weakened the thermal stability of nanofibrous membranes. However, BENF-50 had a higher onset of degradation temperatures and carbon residue rate than those of the other groups, which possibly was due to the optimum interfacial bonding between CA and CS, consistent with our previous report [42]. The ability of the nanofibrous membranes to maintain their porous morphology, structural stability, and thermal stability resulted in

the effective removal of chromium ions from a harsh water environment.

### 3.2 Effects of adsorption performance

The effect of adsorption capacity of the porous biocomposite nanofibrous membranes on  $\text{Cr}^{6+}$  at various contacting time, initial concentrations, and pH values is displayed in Fig. 3. The adsorption capacity of the porous nanofibrous membranes at various ratios increased with increasing time (Fig. 3a). The large specific surface area and functional chemical groups provided both electrostatic adsorption and active chemical sites, which significantly increased the adsorption capacity of the membranes at the initial stages of adsorption ( $t < 60$  min). The adsorption capacity of samples significantly decreased and rapidly reached the adsorption equilibrium except for the BENF-50 and the core-shell-50.

This phenomenon is mainly attributed to decreased  $\text{Cr}^{6+}$  concentration in the solution and declined adsorption sites. The adsorption process was accompanied by the reduction of  $\text{Cr}^{6+}$  to  $\text{Cr}^{3+}$  and the inhibition of further diffusion of  $\text{Cr}^{6+}$  into the nanofibrous membrane. After the adsorption capacities of the membranes reached equilibrium, the samples with the lowest adsorption performance were pure CA and CS nanofibrous membranes corresponding to the adsorption capacities of 5.96 and 9.93 mg/g, respectively. The adsorption capacity of the CA/CS porous membrane increased as the content of CS increased, indicating that CS endowed the membrane with abundant chemical active sites and an excellent and stable network structure. The initial concentration of the  $\text{Cr}^{6+}$  solution was another important factor affecting the adsorption performance. Figure 3b displays the variations in the adsorption capabilities of BENF-50 at various initial  $\text{Cr}^{6+}$  concentrations. The adsorption

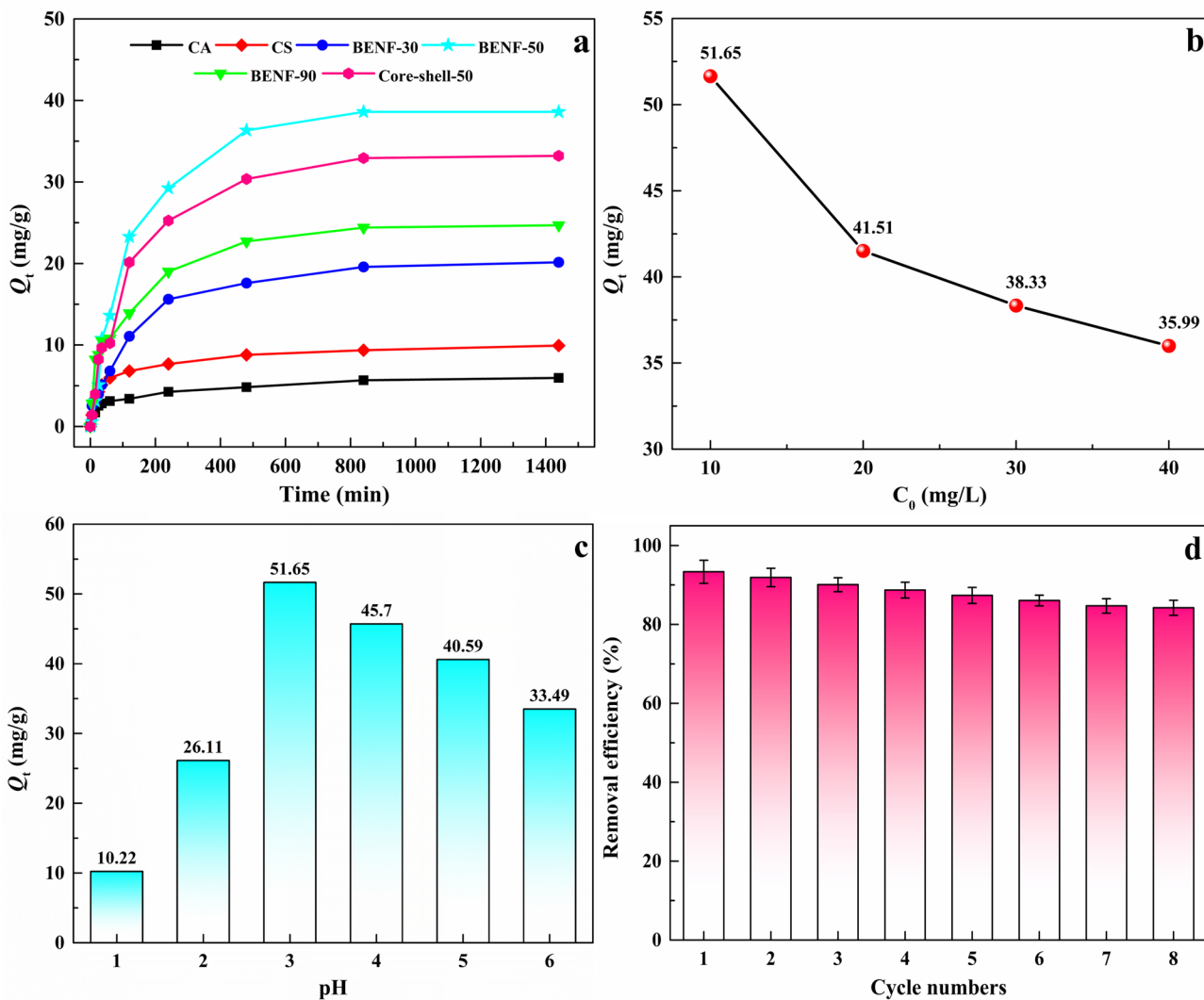


Fig. 3 The effects of time, concentration, pH, and cycle number on the adsorption capacity of chromium ions

capacity of the membrane declined with the increase in initial concentration, especially at 20 mg/L, corresponding to a 19.63% reduction. This result can be attributed to the limited physical and chemical adsorption sites for the increasing amount of  $\text{Cr}^{6+}$  in the solution. The adsorption capacities of the samples were decreased by 7.66% and 6.10% when the concentration of  $\text{Cr}^{6+}$  was further increased to 30 mg/L and 40 mg/L, respectively. A high initial concentration led to the heavy metal ion aggregation on the surface of the membrane. Furthermore, the reduction of  $\text{Cr}^{6+}$  to  $\text{Cr}^{3+}$  bonded to the fiber surface of the biocomposite membrane during the adsorption process, thus preventing the further diffusion of  $\text{Cr}^{6+}$  into the interior of the CA/CS biocomposite membrane.

The pH of the solution with the different surface charges of membranes and the protonation degree of CS also significantly affected the formation of  $\text{Cr}^{6+}$  [43]. Figure 3c illustrates the effects of various pH levels on the  $\text{Cr}^{6+}$  adsorption of CA/CS nanofibrous membranes. The nanofibrous membranes achieved an optimum adsorption capacity of 51.65 mg/g when the pH of the solution was at 3. The  $\text{Cr}^{6+}$  existed in the form of neutral  $\text{H}_2\text{CrO}_4^0$  and negatively charged  $\text{HCrO}_4^-$ ,  $\text{Cr}_2\text{O}_7^{2-}$ , and  $\text{CrO}_4^{2-}$  in acidic solutions [44, 45]. The adsorption capacity of samples significantly improved as the pH value increased from 1 to 3. However, a decreasing adsorption

capacity trend from 51.65 to 33.49 mg/g was observed when the pH value further increased to 6. This can be attributed to the decrease in amino protonation on their surface, thus showing the negative active sites and the weak adsorption of  $\text{HCrO}_4^-$  and  $\text{Cr}_2\text{O}_7^{2-}$  [46]. Eight adsorption–desorption cycle tests were carried out under the experimental conditions of pH=3 and chromium ion solution concentration of 10 mg/L. The adsorbed samples were regenerated in 0.01 M sodium hydroxide for 1 h at room temperature. Figure 3d displays the reusability of the BENF-50 membrane. There was only a little decrease for the adsorption capacity after three cycles with more than 90% removal efficiency. The reduction was about 16% after eight cycles due to the decreasing active sites of amine groups. Overall, the adsorption capacity of CA/CS nanofibrous membranes remained high after eight cycles.

The adsorption mechanism of the CA/CS nanofibrous membranes on chromium ion in different pH solutions is depicted in Fig. 4. The amino groups had electrostatic adsorption interaction with  $\text{HCrO}_4^-$  but an insignificant effect on  $\text{H}_2\text{CrO}_4^0$  when pH=1, leading to the lowest adsorption capacity [40, 47]. The samples exhibited a lower adsorption capacity at pH=2 than at pH=3 due to the strong oxidation of chromate solutions and their susceptibility to redox reactions.  $\text{Cr}^{6+}$  existed in the solution as the octahedral hexahydrionium ion ( $\text{Cr}(\text{H}_2\text{O})_6^{3+}$ ) and was

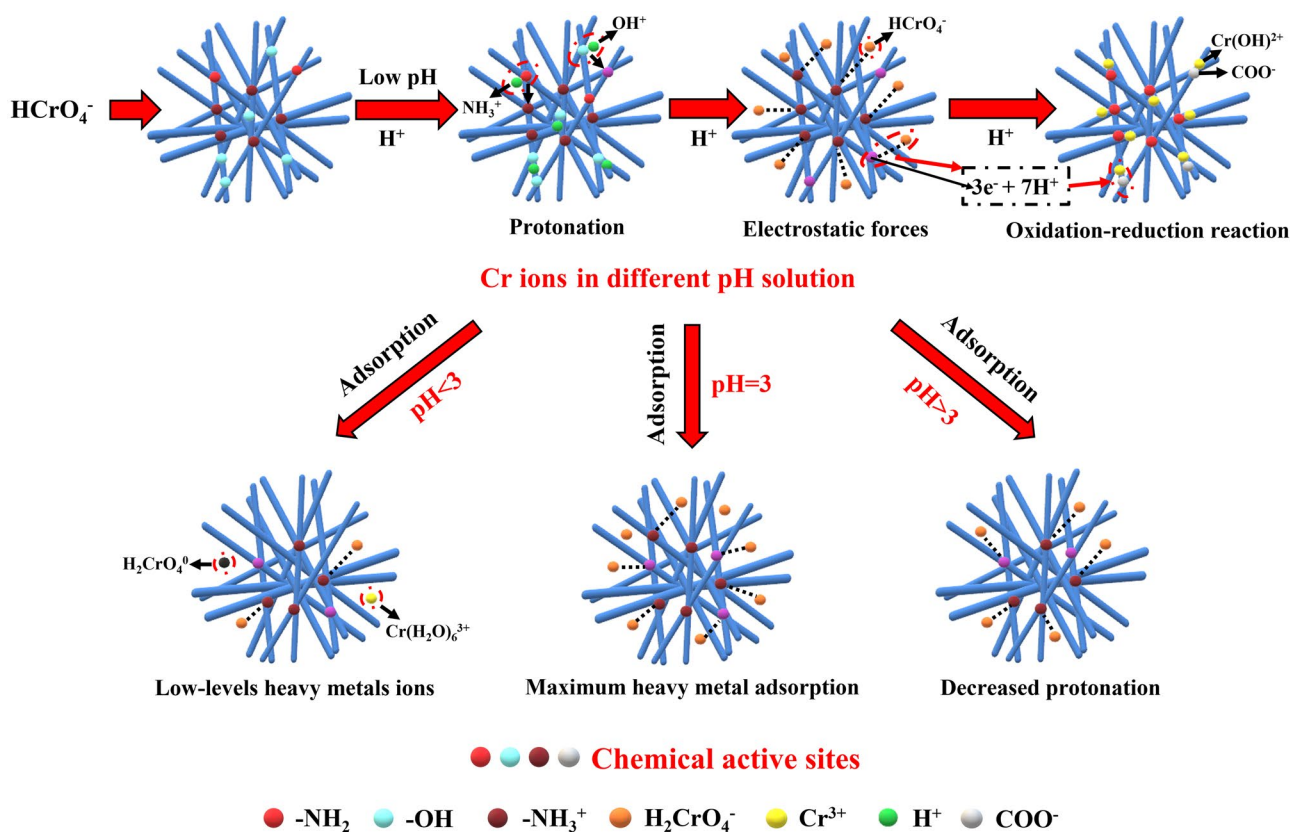


Fig. 4 Chromium ion adsorption mechanism by nanofibrous membranes at various pH values

reduced to  $\text{Cr}^{3+}$  [48]. At  $\text{pH}=3$ , the  $\text{Cr}^{6+}$  solution was mainly dominated by  $\text{HCrO}_4^-$ , which electrostatically attracted the protonated amine, thereby greatly improving the adsorption performance.

### 3.3 SEM-EDS analysis

The adsorbed  $\text{Cr}^{6+}$  SEM-EDS images on porous nanofibrous membranes are depicted in Fig. 5. The SEM observation revealed that many chromate ions ( $\text{Cr}^{6+}$ ) were adsorbed on the membranes made of BENF-30, BENF-50, BENF-90, and core-shell-50 in Fig. 5a1–d1, which was consistent with the EDS analysis result in Fig. 5a3–d3 and Fig. 5a4–d4. The stable network morphology with high porosity endowed the membranes with excellent physical adsorption capacity of chromium ions. The porous CA/CS biocomposite membranes with various CS contents and structures had different adsorption capacities. As shown in Table 1, the chromium ion adsorption capacities of the samples initially increased and then decreased as the contents of CS increased. There was a small amount of chromium ions covered on the surface of BENF-30 in Fig. 5a2. The BENF-50 had the highest chromium ion adsorption capacity (20.51%), with a sufficient

**Table 1** Elemental content of nanofibrous membranes after the adsorption of chromium ions

| Samples       | Element | Weight (%) | Atomic (%) |
|---------------|---------|------------|------------|
| BENF-30       | Cr      | 12.93      | 3.74       |
| BENF-50       | Cr      | 20.51      | 6.48       |
| BENF-90       | Cr      | 10.12      | 2.90       |
| Core-shell-50 | Cr      | 13.41      | 3.97       |

exposure of the CS on the surface of the membrane in Fig. 5b2. However, the BENF-90 with higher CS contents and core-shell-50 with excessive CS exposure on the surface had lower adsorption capacities, possibly corresponding to the weight percentage of 10.12% and 13.41%, which was due to the uneven width distribution of nanofibers and weak structural stability. The dense chromium ions easily destroyed the fine nanofibrous network during the adsorption process, thus deforming whole networks with the emergence of some holes due to the falling of chromium ions in Fig. 5c2 and d2. Therefore, the fabrication of structurally stable nanofibrous membranes with optimum contents of chemically active groups is a prerequisite for effectively bonding heavy metal ions.

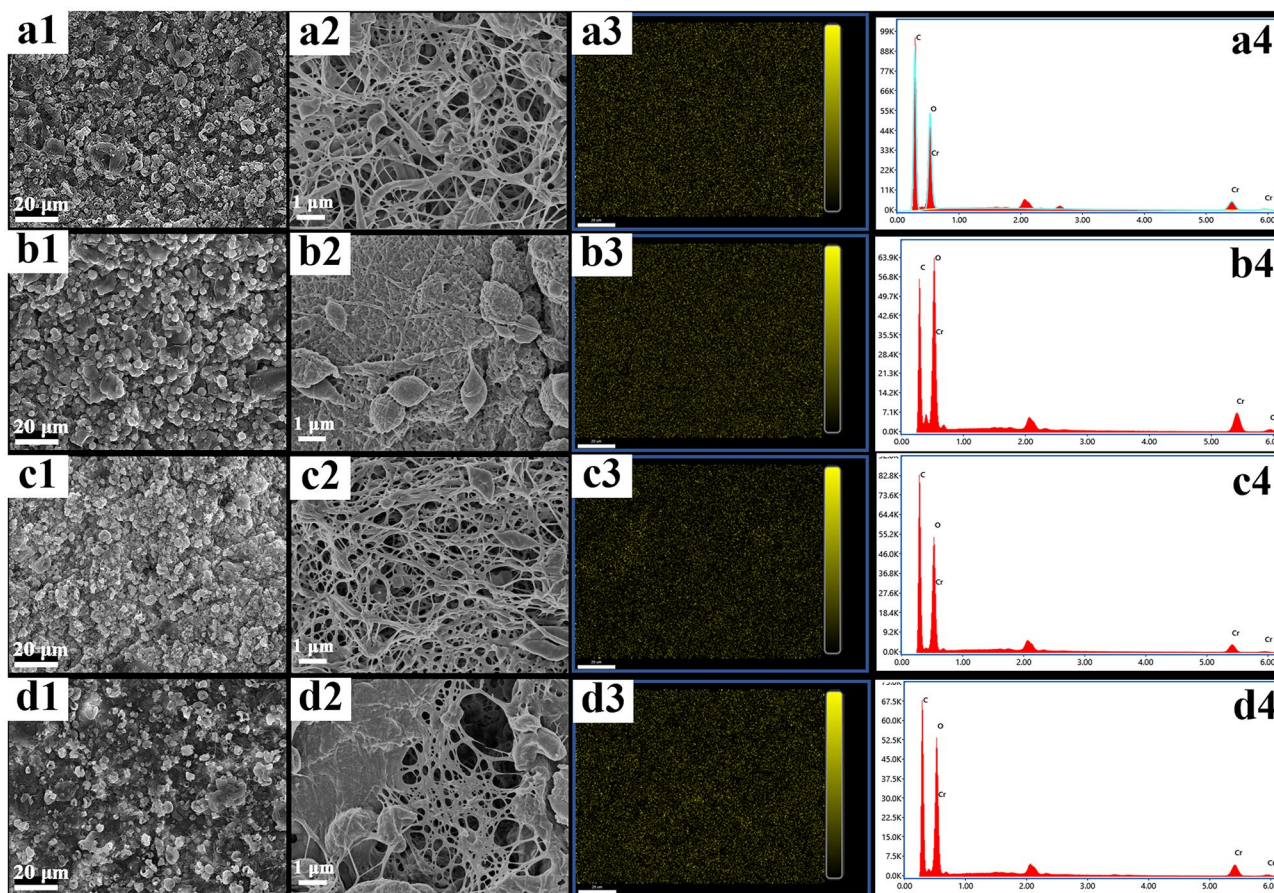


**Fig. 5** SEM-EDS images after the adsorption of chromium ions: **a1–a4** BENF-30, **b1–b4** BENF-50, **c1–c4** BENF-90, and **d1–d4** core-shell-50



### 3.4 Analysis of variation on physical and chemical properties

The XRD patterns and FTIR spectrum of CA/CS biocomposite nanofiber membranes before and after chromium ion adsorption are illustrated in Fig. 6a and b, respectively.

Figure 6a shows that two obvious diffraction peaks appeared at 9.6° and 18.5° were attributed to CA and CS [49, 50]. The peaks can be identified after adsorption of Cr<sup>6+</sup> with the decreasing signal of intensity, which demonstrated the maintenance of ordered structure and amino coordination reaction with Cr<sup>6+</sup>. Figure 6b displays that the

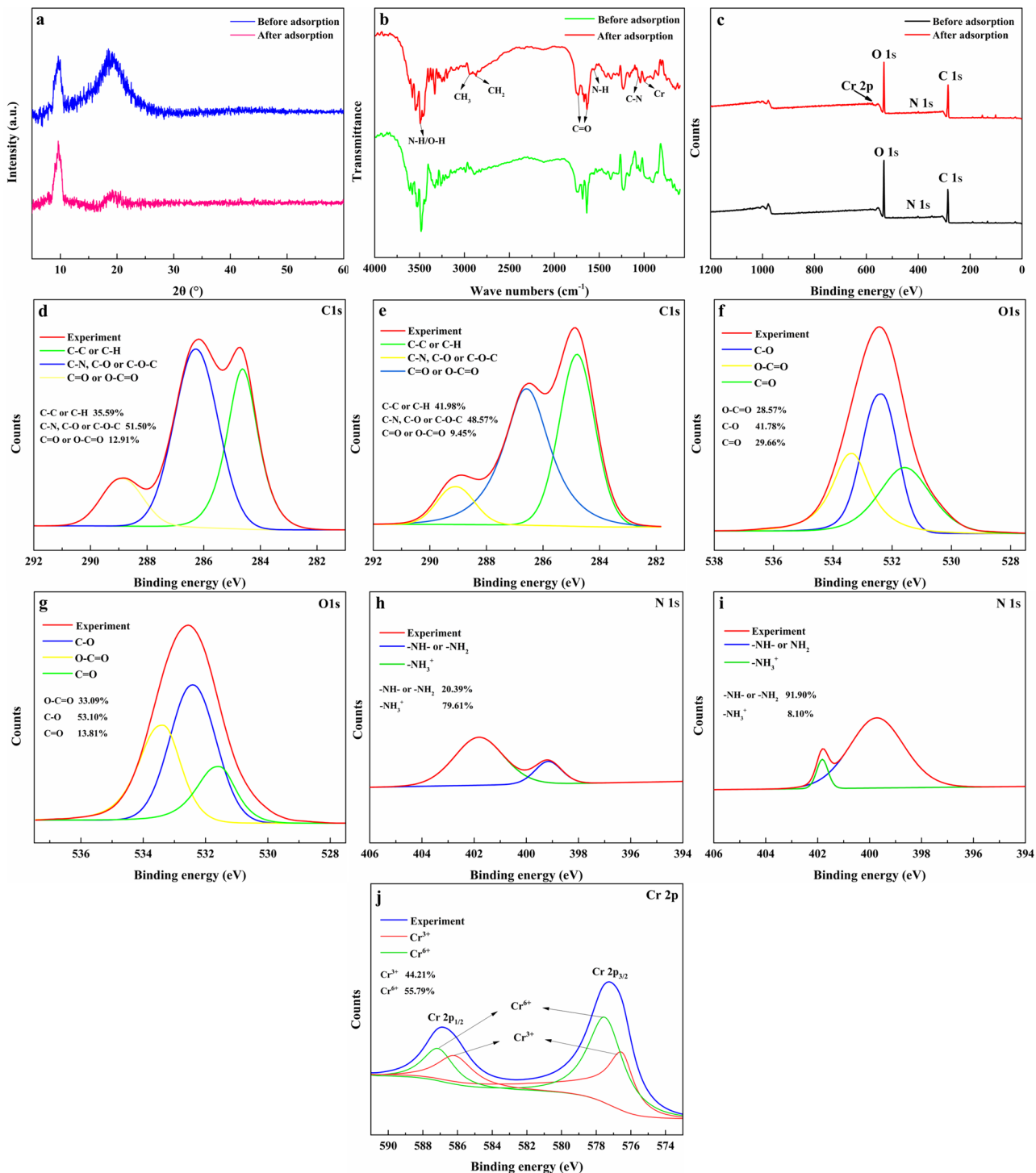


Fig. 6 XRD, FTIR, and XPS spectra of BENF-50 nanofibrous membranes before and after chromium ion adsorption

bands at  $2944\text{ cm}^{-1}$  and  $2890\text{ cm}^{-1}$  were attributed to  $\text{CH}_3$  and  $\text{CH}_2$  stretching vibration in CA and CS. The band at  $1736\text{ cm}^{-1}$  was associated with the stretching vibration of the carbonyl group in CA and the acetyl group in CS [29]. The  $1040\text{ cm}^{-1}$  band was related to the stretching vibration of C–O–C in CS. The  $1636\text{ cm}^{-1}$  band was assigned to the stretching vibration of C–O due to the hydrogen bond [35]. A weak peak appeared at  $1590\text{ cm}^{-1}$ , corresponding to N–H stretching vibration in CS amide II and  $\text{NH}_2$  [51]. The strong adsorption band at  $3490\text{ cm}^{-1}$  corresponds to –OH and –NH stretching vibrations. After the adsorption of  $\text{Cr}^{6+}$ , this peak at  $3491\text{ cm}^{-1}$  was shifted to  $3483\text{ cm}^{-1}$ , probably due to the complexation of –OH groups with  $\text{Cr}^{6+}$  [52]. The appearance of a new peak at  $994\text{ cm}^{-1}$  indicated that the adsorption of  $\text{Cr}^{6+}$  was adsorbed onto the surface of the samples. The peak intensities at  $1635\text{ cm}^{-1}$  were decreased after the adsorption of  $\text{Cr}^{6+}$ ; the decreased peak may be attributed to the complexation between the carboxylic group and  $\text{Cr}^{6+}$  [53]. Another decreased peaks at  $1062\text{ cm}^{-1}$  may be attributed to the interaction of nitrogen from the amino group with  $\text{Cr}^{6+}$  [54]. The characteristic band of C–N at  $1083\text{ cm}^{-1}$  shifted to  $1062\text{ cm}^{-1}$  with the decreasing intensity, indicating the complexation of amine groups with  $\text{Cr}^{6+}$ .

To reveal the chemical adsorption mechanism of CA/CS nanofibrous membranes, XPS analysis was conducted before and after the adsorption of chromium ions, as seen in Fig. 6c. Different atomic states and concentrations of C, O, and N are listed in Table 2. Given the binding energy of C 1s shown in Fig. 6d and e, it was observed that the binding energy of the C–N bonds was shifted from 286.12 to 286.63 eV. This can be speculated that amino groups in CS molecular chains lost the electrons due to the protonation [55]. The O 1s energy spectra in Fig. 6f and g showed that the atomic concentrations of C=O and O–C=O groups decreased after chromium adsorption on BENF-50, which indicated that the hydroxyl groups and residue carbonyl in CA and CS were depleted by the complexation reaction [56]. The N 1s energy spectra are displayed in Fig. 6h and i. Two peaks at 397.72 eV and 399.51 eV were associated with the – $\text{NH}_2$ , –NH–, and protonated – $\text{NH}_3^+$  groups in CS [36, 37]. After the adsorption of  $\text{Cr}^{6+}$ , the binding energies of the two peaks significantly were shifted to 399.70 eV and 401.82 eV, respectively. This suggested that N was involved in the  $\text{Cr}^{6+}$  adsorption process, which was consistent with previous reports [38, 39, 51]. The peak corresponding to the – $\text{NH}_3^+$  binding energy and its intensity became narrower and weaker with lower atomic concentration (0.21%)

**Table 2** The surface elements and functional chemical groups of nanofibrous membranes

| Element                                     | BENF-50<br>before adsorption<br>Binding energy(eV) | BENF-50<br>after adsorption | Assignments                   |
|---|--|-----------------------------|-------------------------------|
| C 1s  | 284.64   | 284.78                      | C–C or C–H                    |
| Atomic concentration (%)                    | 21.83  | 27.42                       |                               |
| C 1s  | 286.12   | 286.63                      | C–N, C–O or C–O–C             |
| Atomic concentration (%)                    | 31.60  | 31.73                       |                               |
| C 1s  | 288.84   | 289.05                      | C=O or O–C=O                  |
| Atomic concentration (%)                    | 7.92   | 6.17                        |                               |
| Total C                                     | 61.36  | 65.04                       |                               |
| O 1s  | 531.57   | 531.64                      | C=O                           |
| Atomic concentration (%)                    | 10.58  | 4.44                        |                               |
| O 1s  | 532.41   | 532.41                      | C–O                           |
| Atomic concentration (%)                    | 14.90  | 17.06                       |                               |
| O 1s  | 533.39   | 533.39                      | O–C=O                         |
| Atomic concentration (%)                    | 10.19  | 10.63                       |                               |
| Total O                                     | 35.66  | 32.04                       |                               |
| N 1s  | 397.72   | 399.70                      | –NH– or –NH <sub>2</sub>      |
| Atomic concentration (%)                    | 0.61   | 2.33                        |                               |
| N 1s  | 399.51   | 401.82                      | –NH <sub>3</sub> <sup>+</sup> |
| Atomic concentration (%)                    | 2.37   | 0.21                        |                               |
| Total N                                     | 2.98   | 2.25                        |                               |
| Cr 2p <sub>3/2</sub> , Cr 2p <sub>1/2</sub> | -  | 576.58, 586.24              | C <sup>3+</sup>               |
| Atomic concentration (%)                    | -  | 0.29                        |                               |
| Cr 2p <sub>3/2</sub> , Cr 2p <sub>1/2</sub> | -  | 577.56, 587.22              | Cr <sup>6+</sup>              |
| Atomic concentration (%)                    | -  | 0.37                        |                               |
| Total Cr                                    | -  | 0.66                        |                               |

after adsorption, implying the involvement of protonated  $-\text{NH}_3^+$  in the electrostatic adsorption process of  $\text{Cr}^{6+}$  [36]. The peak at 399.51 eV with a broader peak width and a significant increase in its intensity and atomic concentration after the adsorption, which was mainly attributed to the conversion of  $\text{Cr}^{6+}$  into  $\text{Cr}^{3+}$  and then adsorbed on the surface of the nanofibrous membrane by the  $-\text{NH}_2$  and  $-\text{NH}-$  groups through electron transfer [36, 40]. In addition, the emergence of two peaks corresponding to 577.28 eV and 586.87 eV in Fig. 6j was respectively assigned to  $\text{Cr } 2p_{3/2}$  and  $\text{Cr } 2p_{1/2}$ , which directly verified that the chromium ions were adsorbed on the surface of the nanofibrous membranes [41, 57]. They were fitted and divided into four specific peaks. The binding energies at 577.6, 587.2 eV, 576.6, and 586.2 eV were associated with  $\text{Cr}^{6+}$  and  $\text{Cr}^{3+}$ , respectively. This demonstrated that  $\text{Cr}^{6+}$  and  $\text{Cr}^{3+}$  co-existed in the nanofibrous membranes, and many  $\text{Cr}^{6+}$  were reduced to  $\text{Cr}^{3+}$  through the redox reaction of existing carboxyl and hydroxyl groups [58].

## 4 Conclusions

The structurally stable nanofibrous biocomposite membranes derived from CA and CS were successfully fabricated using double needles. Nanoindentation mapping revealed that the micro/nano-scale knots were formed through the synergistic action of the hydrogen bonding, electrostatic forces, and interfacial compatibility of CA and CS. The average elastic modulus and hardness values of CA/CS biocomposite nanofibers were 0.23 and 1.72 GPa, respectively. The nanofibrous membrane exhibited outstanding structural stability in aqueous solutions (with a wide pH range) and good thermal stability. The biocomposite nanofibrous membrane containing 50% of CS content had an optimum chromium ion adsorption capacity of 51.6 mg/g in the aqueous solution of pH = 3. The adsorption capacity of CA/CS nanofibrous membranes remained high after eight cycles. The prepared biocomposite nanofibrous membrane exhibited good structural and thermal stabilities as well as excellent adsorption performance, making it a promising adsorption material for water pollution treatment.

**Author contribution** Kaimeng Xu and Guanben Du proposed the scientific target and novelty. Jiayi Wu and Qian Hu performed the experiments for nanofiber fabrication by electrospinning. Jinhui Xiong, Zhiwen Jia, and Lianpeng Zhang helped to complete the operations of SEM-EDS, TG, XPS, FTIR instruments, and the data analyses. Shengbo Ge, Xijuan Chai, and Linkun Xie provided lots of help in discussing the adsorption performance, micro-morphology, and surface chemical composition of nanofibers. Juying Zhou and Yizhong Cao provided a lot of excellent advice on the analysis of the adsorption effect factors and nanoindentation mapping. Yaxin Wang and Jinsong

Yan were responsible for completing all the other experiments. Jinhui Xiong wrote the original draft. Siqun Wang polished the English grammar. Kaimeng Xu, Shengbo Ge, and Guanben Du provided the fund support.

**Funding** The authors sincerely appreciated the financial support of the National Natural Science Foundation of China (NSFC) (32060381), the Applied Basic Research Programs of Yunnan Province (202201AT070058), the National Natural Science Foundation of China (NSFC) (22161043, 32201491), the Opening Project of Guangxi Key Laboratory of Forest Products Chemistry and Engineering, China (GXFK2209), the Scientific Research Funds of Educational Committee of Yunnan Province (2022Y552), National College Students Innovation and Entrepreneurship Training Program (202110677009), the High Level Innovative One-Ten-Thousand Youth Talents of Yunnan Province (YNWR-QNBJ-2020–203), the High-Level Talent Introduction Program of Yunnan Province (YNQR-QNRC-2019–065), and “111” Project (D21027).

## Declarations

**Competing interests** The authors declare no competing interests.

## References

- Si Y, Li J, Cui B, Tang D, Yang L, Murugadoss V, Maganti S, Huang M, Guo Z (2022) Janus phenol–formaldehyde resin and periodic mesoporous organic silica nanoadsorbent for the removal of heavy metal ions and organic dyes from polluted water. *Adv Compos Hybrid Mater* 5:1180–1195. <https://doi.org/10.1007/s42114-022-00446-x>
- Wu Q, Gao L, Huang M, Mersal GA, Ibrahim MM, El-Bahy ZM, Shi X, Jiang Q (2022) Aminated lignin by ultrasonic method with enhanced arsenic (V) adsorption from polluted water. *Adv Compos Hybrid Mater* 5:1044–1053. <https://doi.org/10.1007/s42114-022-00492-5>
- Tshala-Katumbay D, Mwanza J-C, Rohlman DS, Maestre G, Oriá RB (2015) A global perspective on the influence of environmental exposures on the nervous system. *Nature* 527:S187–S192. <https://doi.org/10.1038/nature16034>
- Wu J, Li Q, Su G, Luo R, Du D, Xie L, Tang Z, Yan J, Zhou J, Wang S (2022) Green, ultrafine cellulose-based porous nanofibrous membranes for efficient heavy metal removal through incorporation of chitosan by various electrospinning ways. *Cellulose* 29:5745–5763. <https://doi.org/10.1007/s10570-022-04629-z>
- Zhou Q, Yang N, Li Y, Ren B, Ding X, Bian H, Yao X (2020) Total concentrations and sources of heavy metal pollution in global river and lake water bodies from 1972 to 2017. *Glob Ecol Conserv* 22:e00925. <https://doi.org/10.1016/j.gecco.2020.e00925>
- Zhang Q, Wang C (2020) Natural and human factors affect the distribution of soil heavy metal pollution: a review. *Water Air Soil Poll* 231:1–13. <https://doi.org/10.1007/s11270-020-04728-2>
- Manea YK, Khan AM, Wani AA, Saleh MA, Qashqoosh MT, Shahadat M, Rezakazemi M (2022) In-grown flower like Al-Li/Th-LDH@ CNT nanocomposite for enhanced photocatalytic degradation of MG dye and selective adsorption of Cr (VI). *J Environ Chem Eng* 10:106848. <https://doi.org/10.1016/j.jece.2021.106848>
- Xiao H, Shahab A, Xi B, Chang Q, You S, Li J, Sun X, Huang H, Li X (2021) Heavy metal pollution, ecological risk, spatial distribution, and source identification in sediments of the Lijiang River, China. *Environ Pollut* 269:116189. <https://doi.org/10.1016/j.envpol.2020.116189>
- Azimi A, Azari A, Rezakazemi M, Ansarpour M (2017) Removal of heavy metals from industrial wastewaters: a review. *Chembioeng Rev* 4:37–59. <https://doi.org/10.1002/cben.201600010>

10. Xie X, Gao H, Luo X, Zhang Y, Qin Z, Ji H (2022) Polyethyleneimine-modified magnetic starch microspheres for Cd (II) adsorption in aqueous solutions. *Adv Compos Hybrid Mater* 5:2772–2786. <https://doi.org/10.1007/s42114-022-00422-5>
11. Negahdari S, Sabaghan M, Pirhadi M, Alikord M, Sadighara P, Darvishi M, Nazer M (2021) Potential harmful effects of heavy metals as a toxic and carcinogenic agent in marine food-an overview. *Egypt J Vet* 52:379–385. <https://doi.org/10.21608/ejvs.2021.83716.1245>
12. Benalia MC, Youcef L, Bouaziz MG, Achour S, Menasra H (2022) Removal of heavy metals from industrial wastewater by chemical precipitation: mechanisms and sludge characterization. *Arab J Sci Eng* 47:5587–5599. <https://doi.org/10.1007/s13369-021-05525-7>
13. Razzak SA, Farooque MO, Alsheikh Z, Alsheikhmohamad L, Alkuroud D, Alfayez A, Hossain SZ, Hossain MM (2022) A comprehensive review on conventional and biological-driven heavy metals removal from industrial wastewater. *Environ Adv* 2022:100168. <https://doi.org/10.1016/j.envadv.2022.100168>
14. Peng P, Chen Z, Li X, Wu Y, Xia Y, Duan A, Wang D, Yang Q (2022) Biomass-derived carbon quantum dots modified Bi<sub>2</sub>MoO<sub>6</sub>/Bi<sub>2</sub>S<sub>3</sub> heterojunction for efficient photocatalytic removal of organic pollutants and Cr(VI). *Sep Purif Technol* 291:120901. <https://doi.org/10.1016/j.seppur.2022.120901>
15. Hezarjaribi M, Bakeri G, Sillanpää M, Chaichi MJ, Akbari S, Rahimpour A (2021) New strategy to enhance heavy metal ions removal from synthetic wastewater by mercapto-functionalized hydrous manganese oxide via adsorption and membrane separation. *Environ Sci Pollut R* 28:51808–51825. <https://doi.org/10.1007/s11356-021-14326-2>
16. Sun Y, Zhou S, Pan SY, Zhu S, Yu Y, Zheng H (2020) Performance evaluation and optimization of flocculation process for removing heavy metal. *Chem Eng J* 385:123911. <https://doi.org/10.1016/j.cej.2019.123911>
17. Bashir A, Malik LA, Ahad S, Manzoor T, Bhat MA, Dar G, Pandith AH (2019) Removal of heavy metal ions from aqueous system by ion-exchange and biosorption methods. *Environ Chem Lett* 17:729–754. <https://doi.org/10.1007/s10311-018-00828-y>
18. Pei X, Gan L, Tong Z, Gao H, Meng S, Zhang W, Wang P, Chen Y (2021) Robust cellulose-based composite adsorption membrane for heavy metal removal. *J Hazard Mater* 406:124746. <https://doi.org/10.1016/j.jhazmat.2020.124746>
19. Burakov AE, Galunin EV, Burakova IV, Kucherova AE, Agarwal S, Tkachev AG, Gupta VK (2018) Adsorption of heavy metals on conventional and nanostructured materials for wastewater treatment purposes: a review. *Ecotox Environ Safe* 148:702–712. <https://doi.org/10.1016/j.ecoenv.2017.11.034>
20. Deng Z, Sun S, Li H, Pan D, Patil RR, Guo Z, Seok I (2021) Modification of coconut shell-based activated carbon and purification of wastewater. *Adv Compos Hybrid Mater* 4:65–73. <https://doi.org/10.1007/s42114-021-00205-4>
21. Yin C, Wang C, Hu Q (2021) Selective removal of As (V) from wastewater with high efficiency by glycine-modified Fe/Zn-layered double hydroxides. *Adv Compos Hybrid Mater* 4:360–370. <https://doi.org/10.1007/s42114-021-00214-3>
22. Rehman WU, Khan A, Mushtaq N, Younas M, An X, Saddique M, Farrukh S, Hu Y, Rezakazemi M (2020) Electrospun hierarchical fibrous composite membrane for pomegranate juice concentration using osmotic membrane distillation. *J Environ Chem Eng* 8:104475. <https://doi.org/10.1016/j.jece.2020.104475>
23. Chauque EF, Dlamini LN, Adelodun AA, Greyling CJ, Ngila JC (2016) Modification of electrospun polyacrylonitrile nanofibers with EDTA for the removal of Cd and Cr ions from water effluents. *Appl Surf Sci* 369:19–28. <https://doi.org/10.1016/j.apsusc.2016.02.018>
24. Xu K, Li Q, Xie L, Shi Z, Su G, Harper D, Tang Z, Zhou J, Du G, Wang S (2022) Novel flexible, strong, thermal-stable, and high-barrier switchgrass-based lignin-containing cellulose nanofibrils/chitosan biocomposites for food packaging. *Ind Crop Prod* 179:114661. <https://doi.org/10.1016/j.indcrop.2022.114661>
25. Wang Z, Kang K, Wu J, Hu Q, Harper DP, Du G, Wang S, Xu K (2021) Comparative effects of electrospinning ways for fabricating green, sustainable, flexible, porous, nanofibrous cellulose/chitosan carbon mats as anode materials for lithium-ion batteries. *J Mater Res Technol* 11:50–61. <https://doi.org/10.1016/j.jmrt.2021.01.009>
26. Luo X, Zeng J, Liu S, Zhang L (2015) An effective and recyclable adsorbent for the removal of heavy metal ions from aqueous system: magnetic chitosan/cellulose microspheres. *Bioresource Technol* 194:403–406. <https://doi.org/10.1016/j.biortech.2015.07.044>
27. Ding F, Nie Z, Deng H, Xiao L, Du Y, Shi X (2013) Antibacterial hydrogel coating by electrophoretic co-deposition of chitosan/alkynyl chitosan. *Carbohydr Polym* 98:1547–1552. <https://doi.org/10.1016/j.carbpol.2013.07.042>
28. Ghaee A, Shariaty-Niassar M, Barzin J, Matsuura T (2010) Effects of chitosan membrane morphology on copper ion adsorption. *Chem Eng J* 165:46–55. <https://doi.org/10.1016/j.cej.2010.08.051>
29. Phan DN, Lee H, Huang B, Mukai Y, Kim IS (2019) Fabrication of electrospun chitosan/cellulose nanofibers having adsorption property with enhanced mechanical property. *Cellulose* 26:1781–1793. <https://doi.org/10.1007/s10570-018-2169-5>
30. Zia Q, Tabassum M, Lu Z, Khawar MT, Song J, Gong H, Meng J, Li Z, Li J (2020) Porous poly (L-lactic acid)/chitosan nanofibres for copper ion adsorption. *Carbohydr Polym* 227:115343. <https://doi.org/10.1016/j.carbpol.2019.115343>
31. Christou C, Philippou K, Krasia-Christoforou T, Pashalidis I (2019) Uranium adsorption by polyvinylpyrrolidone/chitosan blended nanofibers. *Carbohydr Polym* 219:298–305. <https://doi.org/10.1016/j.carbpol.2019.05.041>
32. Liu C, Xu D, Weng J, Zhou S, Li W, Wan Y, Jiang S, Zhou D, Wang J, Huang Q (2020) Phase change materials application in battery thermal management system: a review. *Materials* 13:4622. <https://doi.org/10.3390/ma13204622>
33. Seidi F, Shamsabadi AA, Amoghini AE, Saeb MR, Xiao H, Jin Y, Rezakazemi M (2022) Biopolymer-based membranes from polysaccharides for CO<sub>2</sub> separation: a review. *Environ Chem Lett* 20:1083–1128. <https://doi.org/10.1007/s10311-021-01349-x>
34. Liu C, Huang Q, Zheng K, Qin J, Zhou D, Wang J (2020) Impact of lithium salts on the combustion characteristics of electrolyte under diverse pressures. *Energies* 13:5373. <https://doi.org/10.3390/en13205373>
35. Xu C, Cao Y, Chen H, Nie Y, Meng Y, Wu Q, Wang S (2022) Large-scale and high-resolution visualization of static mechanical properties of wood-adhesive interphase utilizing nanoindentation mapping. *Wood Sci Technol* 56:1029–1045. <https://doi.org/10.1007/s00226-022-01394-x>
36. Ren Z, Xu X, Wang X, Gao B, Yue Q, Song W, Zhang L, Wang H (2016) FTIR, Raman, and XPS analysis during phosphate, nitrate and Cr(VI) removal by amine cross-linking biosorbent. *J Colloid Interf Sci* 468:313–323. <https://doi.org/10.1016/j.jcis.2016.01.079>
37. Lv L, Zhang J, Yuan S, Huang L, Tang S, Liang B, Pehkonen SO (2016) Enhanced adsorption of Cu(II) ions on chitosan microspheres functionalized with polyethyleneimine-conjugated poly (glycidyl methacrylate) brushes. *Rsc Adv* 6:78136–78150. <https://doi.org/10.1039/c6ra16226f>
38. Kim MK, Sundaram KS, Iyengar GA, Lee KP (2015) A novel chitosan functional gel included with multiwall carbon nanotube and substituted polyaniline as adsorbent for efficient removal of chromium ion. *Chem Eng J* 267:51–64. <https://doi.org/10.1016/j.cej.2014.12.091>
39. Bhaumik M, Maity A, Srinivasu V, Onyango MS (2012) Removal of hexavalent chromium from aqueous solution using polypyrrole-polyaniline nanofibers. *Chem Eng J* 181:323–333. <https://doi.org/10.1016/j.cej.2011.11.088>

40. Zhao D, Gao X, Wu C, Xie R, Feng S, Chen C (2016) Facile preparation of amino functionalized graphene oxide decorated with  $\text{Fe}_3\text{O}_4$  nanoparticles for the adsorption of Cr(VI). *Appl Surf Sci* 384:1–9. <https://doi.org/10.1016/j.apsusc.2016.05.022>
41. Kumar R, Singh RK, Vaz AR, Savu R, Moshkalev SA (2017) Self-assembled and one-step synthesis of interconnected 3D network of  $\text{Fe}_3\text{O}_4$ /reduced graphene oxide nanosheets hybrid for high-performance supercapacitor electrode. *ACS Appl Mater Inter* 9:8880–8890. <https://doi.org/10.1021/acsami.6b14704>
42. Xu K, Liu C, Kang K, Zheng Z, Wang S, Tang Z, Yang W (2018) Isolation of nanocrystalline cellulose from rice straw and preparation of its biocomposites with chitosan: physicochemical characterization and evaluation of interfacial compatibility. *Compos Sci Technol* 154:8–17. <https://doi.org/10.1016/j.compscitech.2017.10.022>
43. Desbrières J, Guibal E (2018) Chitosan for wastewater treatment. *Polym Int* 67:7–14. <https://doi.org/10.1002/pi.5464>
44. Bhaumik M, Maity A, Srinivasu V, Onyango MS (2011) Enhanced removal of Cr(VI) from aqueous solution using polypyrrole/ $\text{Fe}_3\text{O}_4$  magnetic nanocomposite. *J Hazard Mater* 190:381–390. <https://doi.org/10.1016/j.jhazmat.2011.03.062>
45. Guo L, Zhang Y, Zheng J, Shang L, Shi Y, Wu Q, Liu X, Wang Y, Shi L, Shao Q (2021) Synthesis and characterization of ZnNiCr-layered double hydroxides with high adsorption activities for Cr(VI). *Adv Compos Hybrid Ma* 4:819–829. <https://doi.org/10.1007/s42114-021-00260-x>
46. Yang D, Li L, Chen B, Shi S, Nie J, Ma G (2019) Functionalized chitosan electrospun nanofiber membranes for heavy-metal removal. *Polymer* 163:74–85. <https://doi.org/10.1016/j.polymer.2018.12.046>
47. Avila M, Burks T, Akhtar F, Göthelid M, Lansåker PC, Toprak MS, Muhammed M, Uheida A (2014) Surface functionalized nanofibers for the removal of chromium(VI) from aqueous solutions. *Chem Eng J* 245:201–209. <https://doi.org/10.1016/j.cej.2014.02.034>
48. Zhao R, Li X, Sun B, Li Y, Li Y, Yang R, Wang C (2017) Branched polyethylenimine grafted electrospun polyacrylonitrile fiber membrane: a novel and effective adsorbent for Cr(VI) remediation in wastewater. *J Mater Chem A* 5:1133–1144. <https://doi.org/10.1039/C6TA09784G>
49. Vinodhini PA, Sangeetha K, Thandapani G, Sudha P, Jayachandran V, Sukumaran A (2017) FTIR, XRD and DSC studies of nanochitosan, cellulose acetate and polyethylene glycol blend ultrafiltration membranes. *Chembioeng Rev* 104:1721–1729. <https://doi.org/10.1016/j.ijbiomac.2017.03.122>
50. Habiba U, Siddique TA, Talebian S, Lee JLL, Salleh A, Ang BC, Afifi AM (2017) Effect of deacetylation on property of electrospun chitosan/PVA nanofibrous membrane and removal of methyl orange, Fe (III) and Cr (VI) ions. *Carbohydr Polym* 177:32–39. <https://doi.org/10.1016/j.carbpol.2017.08.115>
51. Wang H, Yuan X, Wu Y, Chen X, Leng L, Wang H, Li H, Zeng G (2015) Facile synthesis of polypyrrole decorated reduced graphene oxide- $\text{Fe}_3\text{O}_4$  magnetic composites and its application for the Cr(VI) removal. *Chem Eng J* 262:597–606. <https://doi.org/10.1016/j.cej.2014.10.020>
52. Singh K, Talat M, Hasan S (2006) Removal of lead from aqueous solutions by agricultural waste maize bran. *Bioresource Technol* 97:2124–2130. <https://doi.org/10.1016/j.biortech.2005.09.016>
53. Xu X, Gao B, Wang W, Yue Q, Wang Y, Ni S (2010) Effect of modifying agents on the preparation and properties of the new adsorbents from wheat straw. *Bioresource Technol* 101:1477–1481. <https://doi.org/10.1016/j.biortech.2009.06.064>
54. Demiral H, Gündüzoğlu G (2010) Removal of nitrate from aqueous solutions by activated carbon prepared from sugar beet bagasse. *Bioresource Technol* 101:1675–1680. <https://doi.org/10.1016/j.biortech.2009.09.087>
55. Wu F, Zhao T, Yao Y, Jiang T, Wang B, Wang M (2020) Recycling supercapacitor activated carbons for adsorption of silver(I) and chromium(VI) ions from aqueous solutions. *Chemosphere* 238:124638. <https://doi.org/10.1016/j.chemosphere.2019.124638>
56. Albadarin AB, Mangwandi C, Walker GM, Allen SJ, Ahmad MN, Khraisheh M (2013) Influence of solution chemistry on Cr(VI) reduction and complexation onto date-pits/tea-waste biomaterials. *J Environ Manage* 114:190–201. <https://doi.org/10.1016/j.jenvman.2012.09.017>
57. Chen L, Zhao D, Chen S, Wang X, Chen C (2016) One-step fabrication of amino functionalized magnetic graphene oxide composite for uranium(VI) removal. *J Colloid Interf Sci* 472:99–107. <https://doi.org/10.1016/j.jcis.2016.03.044>
58. Luo Q, Huang X, Luo Y, Yuan H, Ren T, Li X, Xu D, Guo X, Wu Y (2021) Fluorescent chitosan-based hydrogel incorporating titanate and cellulose nanofibers modified with carbon dots for adsorption and detection of Cr(VI). *Chem Eng J* 407:127050. <https://doi.org/10.1016/j.cej.2020.127050>

**Publisher's Note** Springer Nature remains neutral with regard to jurisdictional claims in published maps and institutional affiliations.

Springer Nature or its licensor (e.g. a society or other partner) holds exclusive rights to this article under a publishing agreement with the author(s) or other rightsholder(s); author self-archiving of the accepted manuscript version of this article is solely governed by the terms of such publishing agreement and applicable law.